ACI MATERIALS JOURNAL TECHNICAL PAPER

Title no. 99-M12

Patch Repair and Macrocell Activity in Concrete Structures

by Franz Pruckner and Odd E. Gjørv

For many years, electrochemical potential mapping has been the most commonly used technique for assessment of steel corrosion in concrete structures. Since the electrochemical potentials are affected by a number of factors, however, a proper interpretation of potential mapping requires much experience. In the present paper, it is shown how a combination of the potential mapping with electrical resistance mapping can reduce both difficulties and uncertainties in the interpretation of potential mapping. By combining so-called net potential differences with concrete resistivities and depths of concrete cover, corrosion activity maps can be produced to visualize the effect of patch repairs on the macrocell activity of localized corrosion on embedded steel. In addition to providing a very good image for assessment of localized corrosion, it is also shown how the severeness of corrosion can be expressed by histograms based on all of the single measurements of galvanic activity.

Keywords: concrete; corrosion; repair.

INTRODUCTION

Over recent years, an increasing amount of premature service life of concrete structures has created a serious problem in many countries. This situation is mostly due to corrosion of embedded steel, where an uncontrolled rate of carbonation or chloride penetration has taken place.[1-3] As soon the corrosion has started, it is often both expensive and technically very difficult to get the corrosion under control. A repair may not necessarily stop the corrosion, and occasionally, the repair may develop galvanic elements in such a way that increased corrosion rates will occur in the structure locally.[4] This is often the case after patch repairs of chloride-induced corrosion have been made.

To make a successful patch repair, a number of considerations should be taken. If the patch only includes the originally anodic and spalled area and chloride-contaminated concrete adjacent to this area is not sufficiently removed, the patch repair may not stop the corrosion. After patching, the effect of the cathodic protection on the adjacent area is lost, and the critical chloride content for initiation of corrosion is reduced. As a consequence, corrosion may start in the adjacent areas. Also, the corrosion rate may be very high because the passive steel surface in the patched area often shows very positive potentials, the effect of which will be a very high driving force.[5]

In the present paper, it is shown how a combination of potential and resistance measurements can be used to visualize the effect of patch repairs on the macrocell activities in concrete structures.

RESEARCH SIGNIFICANCE

Since the electrochemical potentials on embedded steel are affected by a number of factors, a proper interpretation of potential mapping requires much experience. The present paper shows how a combination of the potential mapping with electrical resistance mapping can reduce both difficulties and uncertainties in the interpretation of results and the condition assessment. By producing corrosion activity maps based on net potential differences weighted by the concrete resistivity, a very good image of the macrocell activity of localized corrosion on the embedded steel is obtained. The paper shows how corrosion activity maps can provide a very good basis for assessment of the effect of patch repairs on corroding concrete structures.

THEORETICAL BASIS

Local differences in the chemical properties of the patching material and the adjacent concrete may cause potential differences between various areas of the embedded steel. Such differences will create galvanic macrocells due to the coexistence of passive and corroding areas on the same steel surface. The cell voltage in such a macroelement may give a potential difference between corroding and passive steel of up to 500 mV. The resulting current flow between anodic and cathodic areas can be determined by the electrical resistance of the concrete and the anodic and cathodic reaction resistance as shown in Eq. (1)

$$I = \frac{\Delta U}{R_E + R_A + R_C} \quad (1)$$

where

I = cell current, μA;
ΔU = cell voltage, mV;
R_E = concrete resistance, kΩ;
R_A = anodic reaction resistance, kΩ; and
R_C = cathodic reaction resistance, kΩ.

This current is the result of the electrical field that can be measured along the concrete surface, the result of which is isopotential contours that show the location of corroding zones at the most negative values. Potential mapping is the principal electrochemical technique applied to routine inspection of reinforced concrete structures, the use and interpretation of which are described in ASTM C 876-87 (Table 1).[6]

By taking discrete corrosion potential measurements at regular intervals along the concrete surface, the extent of a corrosion problem can be visualized prior to a more detailed examination and repair. It should be noted, however, that a number of practical conditions may affect the potential readings. Due to inhomogenities in a concrete structure, concentration differences in both moisture and ions may exist. Since positive and negative ions seldom move at the same rate, concentration differences may create potential gradients that

ACI Materials Journal, V. 99, No. 2, March-April 2002.
MS No. 01-087 received March 20, 2001, and reviewed under Institute publication policies. Pertinent discussion will be published in the January-February 2003 *ACI Materials Journal* if received by October 1, 2002.

Franz Pruckner *is a research engineer at Protector Ltd. and a PhD student at the Department of Building Materials at the Norwegian University of Science and Technology, NTNU, Trondheim, Norway. His research interests include electrochemical corrosion of metals in concrete.*

Odd E. Gjørv, *FACI, is a professor of civil engineering at the Department of Building Materials at the University of Science and Technology, NTNU. He is a member of ACI Committees 201, Durability of Concrete; and 222, Corrosion of Metals in Concrete. His research interests include advanced concrete materials and concrete construction as well as durability, maintenance and repairs of concrete structures.*

Table 1—Limiting values for interpretation of electrode potentials[6]

E versus $Cu/CuSO_4$ [mV]	Chance of corrosion
> –200	5%
–200 to –350	Uncertain
< –350	95%

may override the potentials of the embedded steel. This may be more of a problem if the resistivity of the concrete is high.

A carbonation of the outer layer of the concrete may give a shift in potential readings of up to 200 mV, and low availability of oxygen in concrete at high degrees of water saturation may also significantly affect the corrosion conditions. Therefore, a proper interpretation of potential mapping requires much experience.[7]

Combining the potential mapping with resistance mapping can reduce both difficulties and uncertainties in the interpretation of potential mapping. Also, instead of using potential values, net potential differences (NPD) should rather be used as the basis for interpretation.

Based on NPD, concrete resistivities, and depths of concrete cover, it is theoretically possible to determine the rate of galvanic corrosion in the form of weight loss.

The assessment of corrosion rates requires that the ionic current flow in the concrete between areas of noncorroding and corroding steel is calculated, but the calculation of this current from surface potential values requires data on the resistivity of the concrete cover. Based on such data, however, the current flux in a particular region can be obtained.

In the literature, Naish, Harker, and Carney[8] have shown how a corrosion activity map can be derived from potential gradients and resistivity values by use of a finite element model, the result of which is a current flux map as shown in Fig. 1.

The electrical field $\varphi(x,y)$ over a single active/passive macrocell can be determined by the geometry of the system and by the cell voltage ΔU. The cell voltage and the current flowing in the macrocell can then be calculated on the basis of the experimentally measured gradient on the concrete surface.

For a small corrosion cell that is typical for a chloride-induced corrosion, the potential field on the concrete surface can be written as[9,10]

$$\varphi(x,y=d) = \frac{I \cdot \rho}{2\pi \cdot \sqrt{x^2 + d^2}} \text{ [mV]} \qquad (2)$$

where

I = cell current, μA;
ρ = specific concrete resistivity, kΩcm;
d = cover depth, cm; and
x = horizontal distance from the corrosion site, cm.

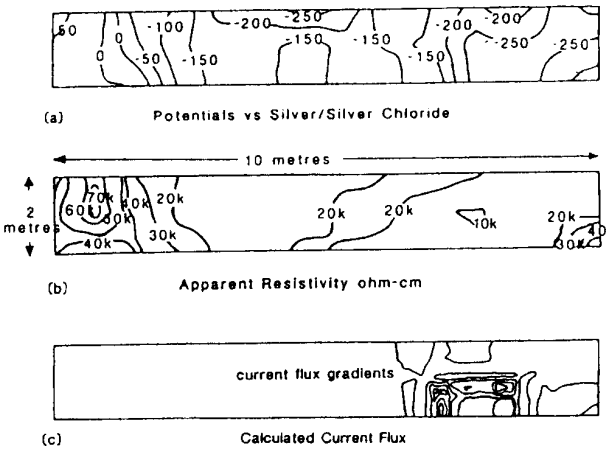

Fig. 1—Derivation of current flux map from potential and resistivity mapping.[8]

The potential difference on the concrete surface between the two points, $x = 0$ and x, can be calculated as

$$\Delta\varphi_x = \varphi(x,d) - \varphi(0,d) = \frac{I \cdot \rho}{2\pi} \cdot \frac{\sqrt{d^2 + x^2} - d}{d \cdot \sqrt{d^2 + x^2}} \qquad (3)$$

from which the current I in the cell is

$$I = \frac{2\pi \cdot \Delta\varphi_x}{\rho} \cdot \frac{d \cdot \sqrt{d^2 + x^2}}{\sqrt{d^2 + x^2} - d} \qquad (4)$$

In the present paper, Eq. (2) has been used to describe the electrical field on the concrete surface for a small corrosion cell, where x describes the lateral distance from the corrosion site. The equation has further been applied to all locations on the concrete surface, where each single location of measurement is treated in relation to the neighboring locations. By knowing the resistivity of the concrete at the place of measurement, it is assumed that galvanic current densities can then be calculated and a corrosion activity map generated.

To obtain information about the electrical field in an electrolyte, the potential difference between two reference electrodes in close vicinity to each other should be measured in a regular grid system. Due to the small currents in the concrete, and also very often due to high electric noise present in the field, such measurements are not very suitable for surveying of concrete structures. As an alternative, therefore, the difference of the measured electrochemical potentials between the point of measurement and its neighboring locations (NPD) is used instead of the electric field. The NPD (weighted by the local resistivity) is believed to represent the net galvanic current absorbed at the location subject to measurement.

For the one-dimensional case of a galvanic couple consisting of mild steel inserted into a rod of stainless steel in 0.5 molar sulfuric acid (Fig. 2), the lateral potential distribution and the NPD are shown in Fig. 3. For the points of equidistant measurements, the NPD for one particular location M is calculated by

$$\text{NPD} = 0.5 \cdot (E_1 + E_2) - E_M \qquad (5)$$

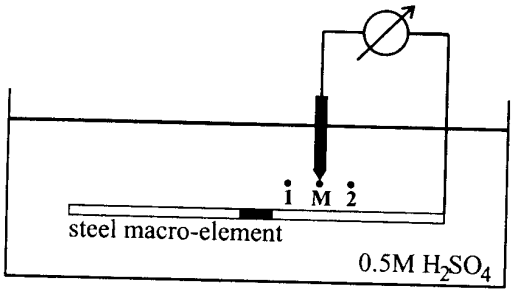

Fig. 2—Experimental setup for measurements of potential distribution of steel macroelement in 0.5 molar sulfuric acid.

where

E_M = potential at location of measurement M; and
E_1, E_2= potentials at neighboring Locations 1 and 2.

It is assumed that the electrolytic resistivity does not vary laterally, and therefore, the NPD should reflect the galvanic activity along the steel macroelement. As can be seen in Fig. 3, the use of NPD gives a much sharper image of the galvanic activity than the lateral distribution of the potential alone. In addition, the values for cathodic and anodic areas are of opposite sign.

For the system steel in concrete, the electrolytic resistivity varies laterally. Therefore, the NPD is weighted by the concrete resistivity for each point of measurement.

If the resistivity of the material is defined as the resistance of a unit-sized cube, the resistivity ρ of a prismatic section with length x and area A is given by

$$\rho = R\frac{A}{x} \tag{6}$$

where R is the resistance of the prismatic section.

To avoid any polarization effects during the measurement, an AC system is used with a frequency in the range of 50 Hz to 1 kHz. The removal of a cylindrical core from the concrete structure each time a resistivity measurement is needed, however, is neither cost-effective nor practical.

The surface technique for measuring electrical resistivity was first used by geologists for investigations of soil and later on applied by Gewertz[11] to a concrete structure in 1958. This technique consists of passing an alternating current between two electrodes in contact with the concrete surface. In a semi-infinite homogeneous material, a flux field is set up, and from a measurement of the potential difference across two other electrodes positioned between the current electrodes, the resistivity of the material can be evaluated. The use of four equispaced electrodes is known as the Wenner array, from which the resistivity is given by

$$\rho = \pi \cdot \frac{U}{I} \cdot \frac{b(b+a)}{a} \tag{7}$$

where

ρ = resistivity, kΩcm;
U/I = resistance, kΩ;
a = inner electrode spacing, cm; and
b = outer electrode spacing, cm.

For the equispaced electrodes in the Wenner array, $a = b$.

For a given type of concrete, the resistivity is mainly related to the moisture content in the concrete and, to a lesser extent, also by the presence of chlorides.[12] In 1958, Gewertz et al.[11] observed that the rate a chloride-induced steel corrosion was negligible for a concrete resistivity above 50 to 70 kΩcm. Table 2 shows the probability of corrosion as a function of the concrete resistivity.

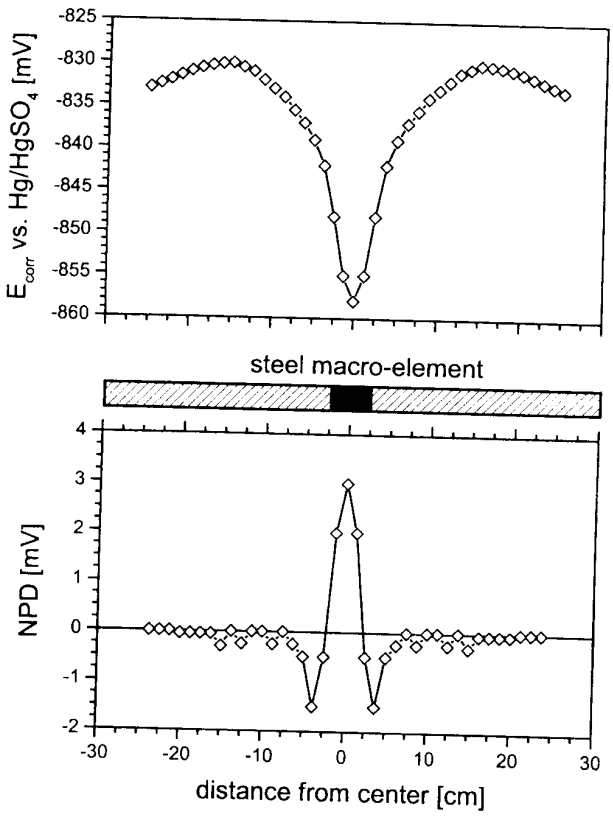

Fig. 3—Lateral potential distribution of corrosion potential and NPD for steel macroelement in 0.5 molar sulfuric acid.

Table 2—Probability of corrosion as a function of concrete resistivity[13]

ρ, kΩcm	Corrosion rate
< 5	Very high
5 to 10	High
10 to 20	Moderate
> 20	Negligible

For the combined measurements of resistivity and potential, Wilkins[14] has suggested to use the same reversible reference electrodes as for the measurement of AC potential differences. In the present work, however, a commercial instrument was used, where the same probe automatically observes both the reinforcing bar potential and the AC resistance between the embedded steel and the probe.[15] The concrete resistivity was then estimated by relating the measured value of cover depth to the area of the surface probe. For calculation of the current flux, Eq. (4) was used in combination with a grid of potential and resistance measurements as shown in Fig. 4.

From the potential measurements, the NPD at Locations E17 and E18, can, for example, be calculated as

$$\mathrm{NPD}_{E17} = \frac{E_{E10} + E_{E16} + E_{E18} + E_{E24}}{4} - E_{E17} \tag{8}$$

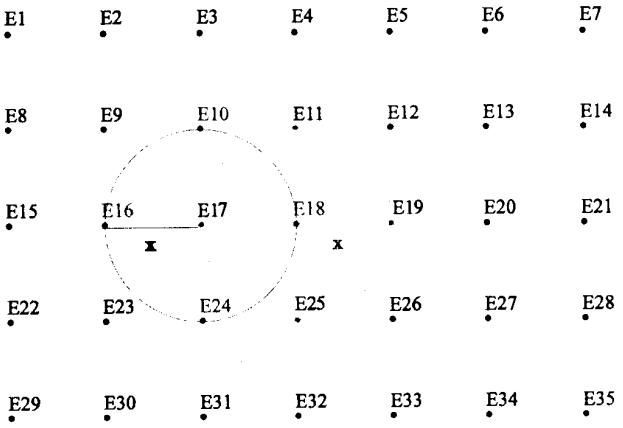

Fig. 4—Grid showing the relative locations of the data points for carrying out potential and resistance mapping also indicating the involved points for creating the corrosion activity map.

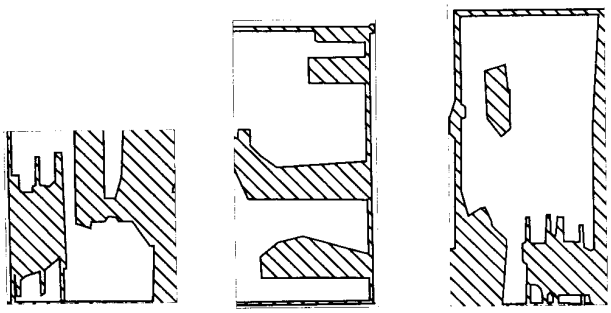

Fig. 5—Patching in Locations A (3.0 × 3.0 m), B (2.5 × 5.0 m), and C (2.75 × 5.25 m).

and

$$\mathrm{NPD}_{E18} = \frac{E_{E11} + E_{E17} + E_{E19} + E_{E25}}{4} - E_{E18}$$

The resistivities (ρ_{E17} and ρ_{E18}) at Locations E17 and E18 were estimated to be approximately the measured resistance, R_{E17} and R_{E18}, multiplied with the area of the electrode surface A, divided by the cover depth d (Eq. (8)). The resistivity was not averaged with values measured at neighboring sites, because for localized corrosion, the conductivity of the medium in close vicinity to the corroding site is limiting the corrosion current

$$\rho_{E17} = R_{E17} \cdot \frac{A}{d} \tag{9}$$

and

$$\rho_{E18} = R_{E18} \cdot \frac{A}{d}$$

FIELD MEASUREMENTS

The combined measurements of potential and resistance values were carried out on the concrete decks of a parking garage that was suffering from chloride-induced corrosion.

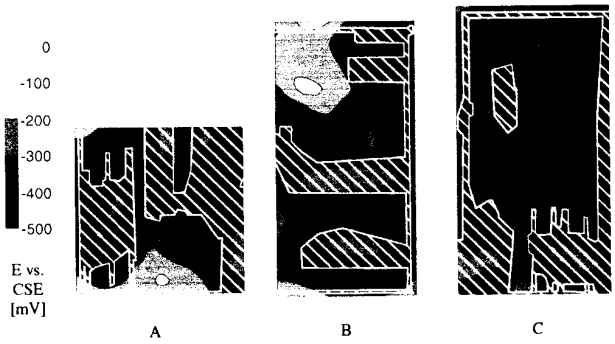

Fig. 6—Isopotential plots for Locations A, B, and C at intervals of 100 mV, from –500 to 0 mV, versus CSE.

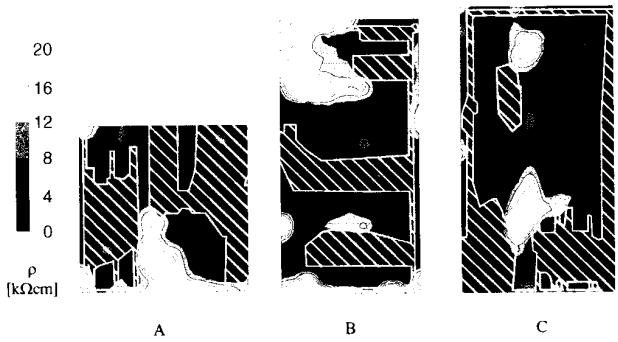

Fig. 7—Isoresistivity plots for Locations A, B, and C at intervals of 4 kΩcm, from 0 to 20 kΩcm.

The decks were going to be rehabilitated by use of cathodic protection (CP), but before the CP system could be applied, extensive patching of the concrete decks had to be carried out. After patching of the concrete decks, three locations for further measurements were selected, the extent of which is shown in Fig. 5.

The potential and resistance mapping was carried out by an instrument of type BLOODHOUND,[15] and the plots were based on intervals of 100 mV for the three locations (Fig. 6). As can be seen, the areas adjacent to the patched areas show the most negative values of corrosion potential compared to the areas in the patches. A possible effect of cathodic protection caused by the corroding reinforcing bars in the old concrete acting as sacrificial anodes might be the reason for pressing the potentials in the patched areas to more negative values. The potentials measured on the reinforcing bars in the patched areas, however, also showed quite negative values. Without knowing the exact location of the patched areas, it would be difficult to find out whether the embedded reinforcing bars were the subject for macrocell corrosion due to the patching or if the corrosion was of a more uniform nature.

From the resistance measurements, a diffuse picture was obtained (Fig. 7). It was not possible to distinguish between repaired areas and nonrepaired areas, which might be due to the fact that the patches were freshly placed at the time of measurement, when the electrolytic conductivity of the patch mortars was still as high as the conductivity of the (chloride-contaminated) concrete surrounding the patches. Measured resistance values were converted to resistivity values by use of Eq. (9).

The most informative image reflecting the corrosion state of the embedded steel was found when the values for the macrocell current density were presented in the form of

corrosion activity maps as shown in Fig. 8. In these maps based on net potential differences weighted by the concrete resistivity, the values of the macrocell current were obtained by use of Eq. (4) and related to the concrete surface area that was covered by each point of measurement.

As can be seen from Fig. 8, it was now easier to distinguish between cathodic and anodic areas of the concrete deck, and the patches generally showed up as cathodic areas as expected, while the anodic areas appeared in the close vicinity of the cathodic patches. These plots support the general experience on how important it is to properly remove all of the chloride-contaminated material from around the corroding areas to reduce the risk of new corrosion in the adjacent areas.

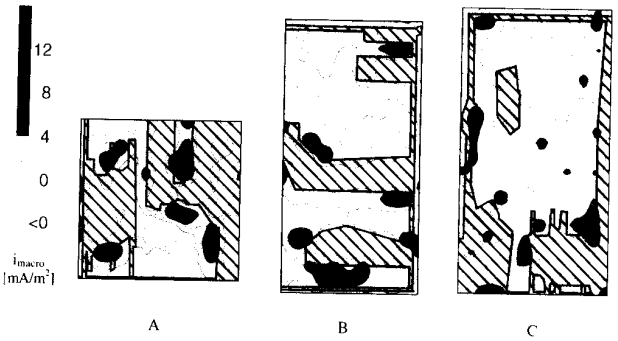

Fig. 8—Plots of macrocell activity in Locations A, B, and C derived from potential and resistance measurements. Galvanic current densities are related to area of concrete surface.

For all the three locations investigated, three-dimensional plots of the macrocell activity are shown in Fig. 9. At discrete places, very high values of anodic activity can be seen, and cathodic areas generally surround these areas. The cathodic areas, on the other hand, do not show as high absolute values as the anodic areas.

For a more uniform corrosion in a concrete structure without any local differences in the electrochemical potential, a more flat map of macrocell activity would probably be obtained. Also, the values of corrosion activity would probably be in the vicinity of zero.

When further analyzing the values of corrosion activity in the form of histograms based on all single measurements of macrocell activity, Fig. 10 shows that a significant amount of the single values are located in the high positive region. The distribution is not symmetric at zero, but it flattens out more slowly towards the positive values. For a more uniform corrosion, the curve would probably be more symmetric with a more narrow width and higher amplitude at zero. However, for a more localized corrosion, as in the present case, the curve is still distributed around zero, but the sites of localized corrosion are reflected in the form of an asymmetric peak. The much lower and more uniform current densities for the cathodic compared with those of the anodic sites may be due to the fact that the cathodic reaction (oxygen reduction) was more uniform than localized.

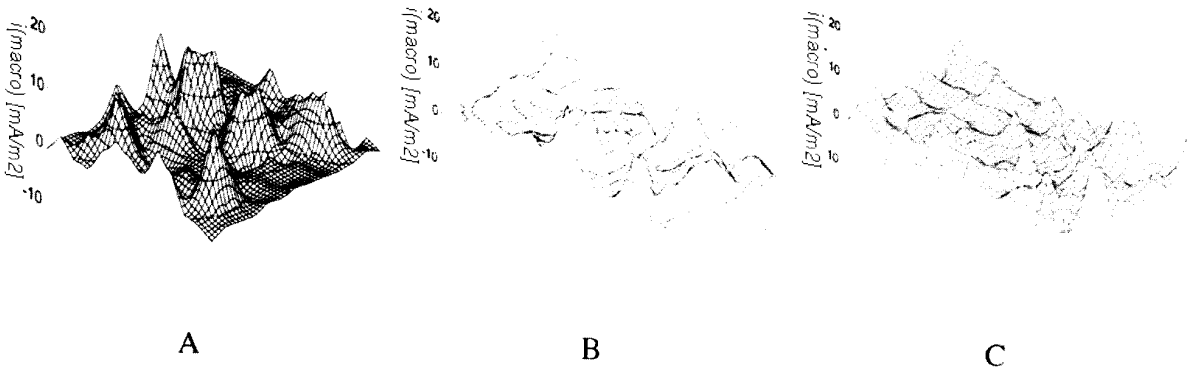

Fig. 9—Three-dimensional plots of macrocell activity in Locations A, B, and C.

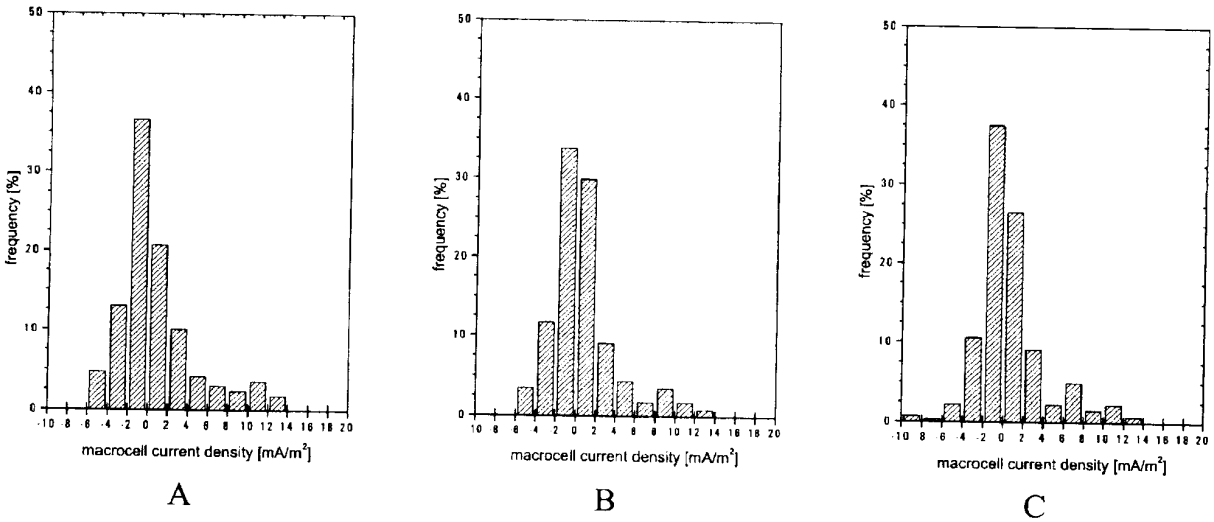

Fig. 10—Histograms based on all single values of galvanic activity in Locations A, B, and C.

CONCLUSIONS

On the basis of the research program presented in the present paper, the following conclusions appear to be warranted:

1. Corrosion activity maps based on net potential differences weighted by the concrete resistivity appear to provide a very good image of the macrocell activity of localized corrosion on embedded steel in concrete;

2. Through the use of corrosion activity maps, both more information and more accurate information about the state of corrosion can be obtained compared with that of conventional potential mapping;

3. The severeness of a localized corrosion activity can be expressed by histograms based on all single measurements of macrocell activity;

4. The treatment and analysis of data presented in the represented paper can easily be implemented in the software system for existing mapping equipment; and

5. For further work, a comparison of corrosion activity maps measured on a large number of objects in combination with destructive test methods may lead to an improved standard for interpretation of the nondestructive techniques for potential and resistivity mapping.

ACKNOWLEDGMENTS

The authors greatly acknowledge the financial support received from Protector AS.

REFERENCES

1. Comptroller General of the United States, "Solving Corrosion Problems of Bridge Surfaces Could Save Billions," United States General Accounting Office PSAD-79-10, 1979.

2. American Association of State Highway and Transportation Officials, "Strategic Highway Research Program—Research Plans," Transportation Research Board, 1986.

3. Gjørv, O. E., "Steel Corrosion in Concrete Structures Exposed to Norwegian Marine Environment," *Concrete International*, V. 16, No. 4, Apr. 1994, pp. 35-39.

4. Wheat, H. G., and Harding, K. S., "Galvanic Corrosion in Repaired Reinforced Concrete Slabs—An Update," *Materials Performance*, V. 5, 1993, pp. 58-62.

5. Raupach, M., "Chloride-Induced Macrocell Corrosion of Steel in Concrete—Theoretical Background and Practical Consequences," *Construction and Building Materials*, V. 10, 1996, pp. 329-338

6. ASTM C 876-87, "Half-Cell Potentials of Uncoated Steel in Concrete," ASTM, West Conshohocken, Pa., 1987.

7. Francois, R.; Arliguie, G.; and Bardie, D., "Electrode Potential Measurements of Concrete Reinforcement for Corrosion Evaluation," *Cement and Concrete Research*, V. 24, 1994, pp. 401-412.

8. Naish, C. C.; Harker, A.; and Carney, R. F. A., "Concrete Inspection: Interpretation of Potential and Resistivity Measurements," *Corrosion of Reinforcement in Concrete*, C. L. Page, K. W. J. Treadaway, and P. B. Bamforth, eds., Elsevier, 1990, pp. 314-332.

9. Elsener, B., and Böhni, H., "Potential Mapping and Corrosion of Steel in Concrete," *Corrosion Rates of Steel in Concrete*, N. S. Berke, V. Chaker, and D. Whiting, eds., ASTM, West Conshohocken, Pa., 1990, pp. 143-156.

10. Baeckmann, W.; Schwenk, W.; and Prinz, W., "Handbuch des Kathodischen Korrosionsschutzes," *Verlag Chemie*, Weinheim, 1989, 120 pp.

11. Gewertz, M. W.; Tremper, B.; Beaton, J. L.; and Stratfull, R. F., "Causes and Repair of Deterioration to a Californian Bridge due to Corrosion of Reinforcing Steel in a Marine Environment," *Highway and Research Board Bulletin* 182, 1958, 41 pp.

12. Gjørv, O. E.; Vennesland, Ø.; and El-Bussaidy, A. H. S., "Electrical Resistivity of Concrete in Oceans," *Paper* OTC 2803, Offshore Technology Conference, May 1977, Houston, Tex., pp. 581-588.

13. Brown, R. R., and Rockock, D. C., "Assessment in Practice," Comett Course Aachen, 1992.

14. Wilkins, N. J. M., "Resistivity of Concrete," AERE-M 3232, 1982.

15. "BLOODHOUND," Potential and Resistance Mapping Device, Cyberdan A/S, Denmark.